Polarization-gratings approach to deformed-helix ferroelectric liquid crystals with subwavelength pitch

Alexei D. Kiselev,[1,2,*] Eugene P. Pozhidaev,[3,2,†] Vladimir G. Chigrinov,[2,‡] and Hoi-Sing Kwok[2,§]
[1]*Institute of Physics of National Academy of Sciences of Ukraine, Prospekt Nauki 46, 03028 Kyïv, Ukraine*
[2]*Hong Kong University of Science and Technology, Clear Water Bay, Kowloon, Hong Kong*
[3]*P.N. Lebedev Physics Institute of Russian Academy of Sciences, Leninsky Prospect 53, 117924 Moscow, Russia*
(Received 19 December 2010; published 18 March 2011)

Electro-optical properties of deformed helix ferroelectric liquid crystal (DHFLC) cells are studied by using a general theoretical approach to polarization gratings in which the transmission and reflection matrices of diffraction orders are explicitly related to the evolution operator of equations for the Floquet harmonics. In the short-pitch approximation, a DHFLC cell is shown to be optically equivalent to a uniformly anisotropic biaxial layer where one of the optical axes is normal to the bounding surfaces. For in-plane anisotropy, orientation of the optical axes and birefringence are both determined by the voltage applied across the cell and represent the parameters that govern the transmittance of normally incident light passing through crossed polarizers. We calculate the transmittance as a function of the electric field and compare the computed curves with the experimental data. The theoretical and experimental results are found to be in good agreement.

DOI: 10.1103/PhysRevE.83.031703 PACS number(s): 61.30.Gd, 61.30.Hn, 77.84.Nh, 42.79.Kr

I. INTRODUCTION

A *polarization grating* (PG) can generally be described as an optically anisotropic layer characterized by the anisotropy parameters that periodically vary in space along a line in the plane of its input face. Unlike conventional phase and amplitude diffraction gratings, PGs act by locally modifying the polarization state of light waves passing through them. Owing to the one-dimensional (1D) in-plane periodicity, this introduces periodically modulated changes of the polarization characteristics giving rise to polarization-dependent diffraction. In particular, the latter implies that a PG divides a monochromatic plane wave into differently polarized diffracted waves.

Over the past decade PGs have been attracted much attention due to a unique combination of their optical properties: (a) it is possible to achieve 100% diffraction into a single order; (b) diffraction efficiencies are highly sensitive to the incident light polarization; and (c) the state of polarization of diffracted orders is determined solely by the parameters of a PG [1–4]. There are numerous applications in a variety of fields, including polarimeters, displays, polarizing beam splitters, beam steering, and polarization multiplexers where PGs have been found to be useful (for recent reviews, see the articles [5–7] and the monograph [8]).

There are different technologies to fabricate PGs. For example, computer-generated subwavelength-period metal-stripe gratings with spatially periodic fringe orientation [9] and space-variant dielectric subwavelength gratings formed by discrete orientation of local subwavelength grooves [10,11] are produced using advanced photolithographic and etching techniques. Such gratings were employed to perform real-time polarization measurements [10–12]. They were also used to demonstrate polarization Talbot self-imaging [13] and Pancharatnam-Berry phase optical elements [14,15].

Polarization holography provides another well-known method to produce PGs [8]. It uses two differently polarized light beams to record the spatially modulated polarization state of the resultant light field on suitable media such as azobenzene containing polymer systems and silver-halide materials.

The holographic technique has been extensively used to create PGs in liquid crystal (LC) cells with photosensitive aligning substrates such as linear photopolymerizable polymer layers [16,17], azo-dye films [18], azo-dye doped polyimide [19,20], and azobenzene side-chain polymer layers [21].

In this method, irradiation of the substrate with a holographically generated polarization interference pattern gives rise to spatially modulated light induced ordering in the photoaligning layer. This ordering manifests itself in the effect of photoinduced optical anisotropy and determines the anchoring properties of the layer such as its (polar and azimuthal) anchoring strengths and the easy axis orientation (see, e.g., Refs. [22–24] and references therein).

The anchoring parameters of the photoaligning film thus undergo periodic variations across the substrate face leading to the formation of orientational structures in the LC cells [25] characterized by spatially periodic distributions of the LC director, $\hat{\mathbf{d}} = (d_x, d_y, d_z)$, which is a unit vector that defines a local direction of the preferential orientation of LC molecules. In LCs, the elements of the dielectric tensor, ε, can be expressed in terms of the LC director [26],

$$\epsilon_{ij} = \epsilon_\perp(\delta_{ij} + u_a\, d_i\, d_j), \quad u_a = (\epsilon_\parallel - \epsilon_\perp)/\epsilon_\perp, \tag{1}$$

where δ_{ij} is the Kronecker symbol, u_a is the *anisotropy parameter*, and $n_\perp \equiv n_o = \sqrt{\mu\epsilon_\perp}$ ($n_\parallel \equiv n_e = \sqrt{\mu\epsilon_\parallel}$) is the ordinary (extraordinary) refractive index (the magnetic tensor of LC is assumed to be isotropic with the magnetic permittivity μ). So, the periodic orientational LC configurations define the so-called *liquid crystal polarization gratings* (LCPGs). These gratings are our primary interest.

*kiselev@iop.kiev.ua
†epozhidaev@mail.ru
‡eechigr@ust.hk
§eekwok@ust.hk

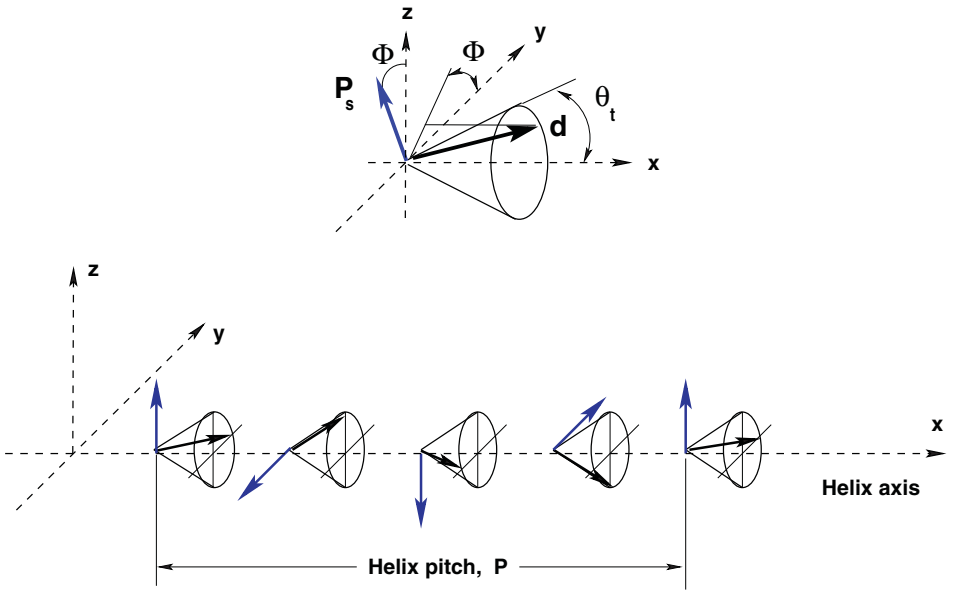

FIG. 1. (Color online) Helical structure of deformed helix ferroelectric liquid crystals. The FLC director, $\hat{\mathbf{d}}$, lies on the smectic cone with cone angle θ_t and rotates around the helix axis (the x axis) along with the vector of the spontaneous ferroelectric polarization, $\mathbf{P}_s$.

Common methods most generally employed to derive theoretical results for PGs typically rely on the well-known Jones matrix formalism and its modifications [1–5,8–11,21]. These results are limited by their assumptions to large gratings periods and normal incidence. In addition, using Jones calculus implies neglecting multiple reflections.

In this work we present the theoretical approach to PGs that can be regarded as a generalized version of our method developed in Refs. [27,28] for stratified anisotropic media and goes beyond the limitations of Jones calculus. We apply the method for systematic treatment of the technologically important case of the deformed helix ferroelectric liquid crystals (DHFLCs) [29,30], where the LC director rotates about a uniform twist axis parallel to the substrates forming the ferroelectric LC (FLC) helical structure (see Fig. 1).

In DHFLC cells, the FLC helix is characterized by a short submicron *helix pitch*, $P < 1\ \mu$m, and a relatively large *tilt angle*, $\theta_t > 30^\circ$. Note that, in the case of surface stabilized FLC cells, the helix pitch of a FLC mixture is typically greater than the cell thickness, so that the bulk chiral helix turned out to be suppressed by the boundary conditions at the substrates [31]. By contrast to this, a DHFLC helix pitch is 5–10 times smaller than the thickness. This allows the helix to be retained within the cell boundaries.

Electro-optical response of DHFLC cells exhibits a number of peculiarities that make them useful for LC devices such as high-speed spatial light modulators [32–34] and color-sequential LC display cells [35]. So, in this study, our goal is to examine electro-optical properties of DHFLCs based on the general theoretical approach describing PGs.

The layout of the paper is as follows.

In Sec. II we begin with Maxwell's equations for the lateral components of the electric and magnetic fields and derive a set of equations for the Floquet harmonics representing diffracted waves. The relations linking the transmission and reflection matrices of diffraction orders and the evolution operator of the system for the harmonics are deduced in Sec. II C.

Electro-optical properties of DHFLC cells with the sub-wavelength helix pitch are studied in Sec. III. Experimental details are given in Sec. III A, where we describe the samples and the setup employed to perform measurements. In Sec. III B, the general theory of Sec. II is used to examine how the optical anisotropy parameters and the transmission coefficients of the DHFLC cells depend on the applied electric field. In particular, it is found that in the short-pitch approximation the DHFLC PGs can be represented by uniformly anisotropic biaxial layers. For the electric field dependence of the light transmittance through the cell placed between crossed polarizers, the results of electro-optical measurements are compared with the theoretically computed curves in Sec. III C.

Finally, in Sec. IV, we present the results and make some concluding remarks. Technical details on the derivation of Maxwell's equations for the lateral (in-plane) components of the electromagnetic field are relegated to the Appendix.

II. THEORY OF POLARIZATION GRATINGS

In this section we generalize the theoretical approach developed in Refs. [27,28] so as to treat the light transmission problem for a PG in the slab geometry shown in Fig. 2. In this geometry, as is indicated in Fig. 2, the z axis is normal to the bounding surfaces of the layer: $z = 0$ and $z = D$, the grating with the *grating pitch*, Λ_g, and the *grating wave vector*,

$$\mathbf{k}_g = k_g \hat{\mathbf{x}}, \quad k_g = \frac{2\pi}{\Lambda_g}, \tag{2}$$

where k_g is the *grating wave number*, is characterized by the condition of in-plane periodicity for the elements of the dielectric tensor, $\boldsymbol{\epsilon}$:

$$\epsilon_{ij}(x + \Lambda_g) = \epsilon_{ij}(x). \tag{3}$$

Expression for the grating wave vector (2) defines the x-z plane as the *plane of grating*.

Throughout this paper we deal with harmonic electromagnetic fields characterized by the *frequency*, ω (time-dependent factor is $\exp\{-i\omega t\}$), and the *free-space wave number*, $k_{\text{vac}} = \omega/c$. So, the starting point of our theoretical considerations is

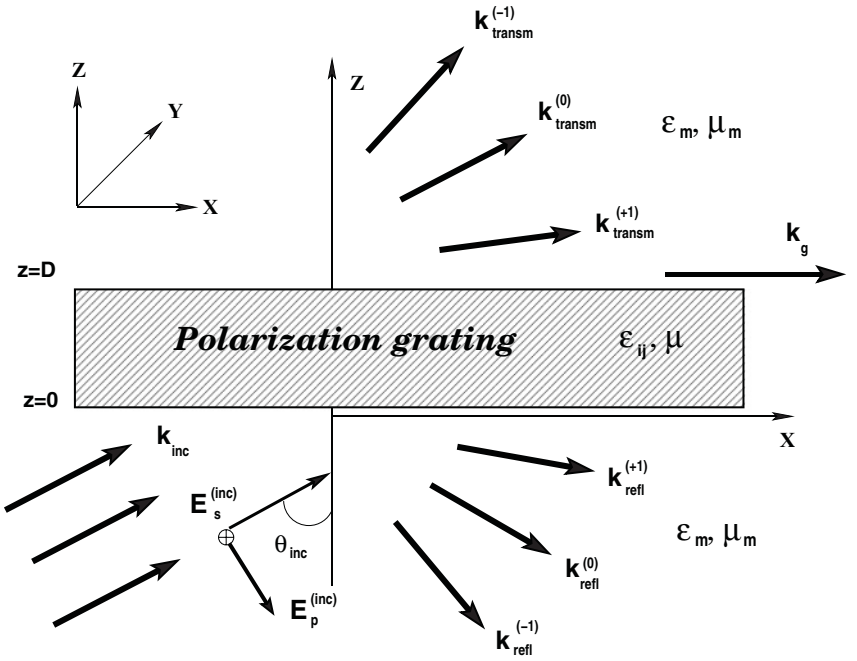

FIG. 2. Schematic representation of slab geometry in the plane of PG with the grating wave vector $\mathbf{k}_g$. The incident wave with the wave vector $\mathbf{k}_{\rm inc}$ impinges onto the gratings and the diffraction orders of reflected (transmitted) waves are characterized by the wave vectors $\mathbf{k}_{\rm refl}^{(0)}$ and $\mathbf{k}_{\rm refl}^{(\pm 1)}$ ($\mathbf{k}_{\rm trm}^{(0)}$ and $\mathbf{k}_{\rm trm}^{(\pm 1)}$).

the Maxwell equations for a harmonic electromagnetic wave written in the form

$$\nabla \times \mathbf{E} = i\mu k_{\rm vac}\mathbf{H}, \tag{4a}$$

$$\nabla \times \mathbf{H} = -ik_{\rm vac}\mathbf{D}, \tag{4b}$$

where $\mathbf{D} = \boldsymbol{\varepsilon} \cdot \mathbf{E}$ is the electric displacement field.

We also assume (see Fig. 2) that the medium surrounding the layer is optically isotropic with the dielectric constant $\epsilon_{\rm m}$, the magnetic permittivity $\mu_{\rm m}$, and the refractive index $n_{\rm m} = \sqrt{\mu_{\rm m}\epsilon_{\rm m}}$. So, for a plane wave traveling along the wave vector

$$\mathbf{k} = k_{\rm m}\hat{\mathbf{k}} = k_z\hat{\mathbf{z}} + \mathbf{k}_p, \quad \mathbf{k}_p = k_p[\cos(\phi)\,\hat{\mathbf{x}} + \sin(\phi)\,\hat{\mathbf{y}}],$$
$$k_{\rm m} = n_{\rm m}k_{\rm vac}, \tag{5}$$

the electromagnetic field $\{\mathbf{E},\mathbf{H}\}$ is given by

$$\{\mathbf{E},\mathbf{H}\} = \{\mathbf{E}(\hat{\mathbf{k}}),\mathbf{H}(\hat{\mathbf{k}})\}\exp[i(\mathbf{k}\cdot\mathbf{r})], \tag{6a}$$

$$\mathbf{E}(\hat{\mathbf{k}}) = E_p\,\mathbf{e}_x(\hat{\mathbf{k}}) + E_s\,\mathbf{e}_y(\hat{\mathbf{k}}), \tag{6b}$$

$$\frac{\mu_{\rm m}}{n_{\rm m}}\mathbf{H}(\hat{\mathbf{k}}) = \hat{\mathbf{k}} \times \mathbf{E}(\hat{\mathbf{k}}) = E_p\,\mathbf{e}_y(\hat{\mathbf{k}}) - E_s\,\mathbf{e}_x(\hat{\mathbf{k}}), \tag{6c}$$

where the unit vectors $\hat{\mathbf{k}} = (\sin\theta\cos\phi, \sin\theta\sin\phi, \cos\theta)$, $\mathbf{e}_x(\hat{\mathbf{k}}) = (\cos\theta\cos\phi, \cos\theta\sin\phi, -\sin\theta)$, and $\mathbf{e}_y(\hat{\mathbf{k}}) = (-\sin\phi, \cos\phi, 0)$, expressed in terms of the polar (θ) and azimuthal (ϕ) angles form an orthogonal basis.

The incoming incident wave $\{\mathbf{E}_{\rm inc},\mathbf{H}_{\rm inc}\}$ is represented by a plane wave (6), $\{\mathbf{E},\mathbf{H}\} = \{\mathbf{E}_{\rm inc},\mathbf{H}_{\rm inc}\}$, propagating along the wave vector,

$$\mathbf{k} = \mathbf{k}_{\rm inc} = k_z^{\rm (inc)}\hat{\mathbf{z}} + \mathbf{k}_p, \quad k_z^{\rm (inc)} = \sqrt{k_{\rm m}^2 - k_p^2}, \tag{7}$$

in the half space $z \leqslant 0$ bounded by the input face of the grating. In this case, the polar angle, $0 \leqslant \theta = \theta_{\rm inc} < \pi/2$, is the *angle of incidence*, whereas the azimuthal angle, $0 \leqslant \phi = \phi_{\rm inc} < 2\pi$, is the angle between the grating plane and the *plane of incidence*.

A. Maxwell's equations for lateral components

Now we write down the representation for the electric and magnetic fields, $\mathbf{E}$ and $\mathbf{H}$,

$$\mathbf{E} = E_z\hat{\mathbf{z}} + \mathbf{E}_P, \quad \mathbf{H} = H_z\hat{\mathbf{z}} + \hat{\mathbf{z}} \times \mathbf{H}_P, \tag{8}$$

where the components directed along the normal to the bounding surface (the z axis) are separated from the tangential (lateral) ones. In this representation, the vectors

$$\mathbf{E}_P = E_x\hat{\mathbf{x}} + E_y\hat{\mathbf{y}} \equiv \begin{pmatrix} E_x \\ E_y \end{pmatrix}$$

and

$$\mathbf{H}_P = \mathbf{H} \times \hat{\mathbf{z}} \equiv \begin{pmatrix} H_y \\ -H_x \end{pmatrix}$$

are parallel to the substrates and give the lateral components of the electromagnetic field. Similar decomposition for the differential operator that enter the Maxwell equations (4) is given by

$$k_{\rm vac}^{-1}\nabla = \hat{\mathbf{z}}\,\partial_\tau + i\nabla_p, \quad \nabla_p^{\perp} = \hat{\mathbf{z}} \times \nabla_p, \tag{9}$$

where $\tau = k_{\rm vac}z$; $\nabla_p = -i\,k_{\rm vac}^{-1}(\hat{\mathbf{x}}\,\partial_x + \hat{\mathbf{y}}\,\partial_y) \equiv (\nabla_x, \nabla_y)$ and $\nabla_p^{\perp} = (\nabla_x^{\perp}, \nabla_y^{\perp}) = (-\nabla_y, \nabla_x)$.

We can now substitute Eqs. (8) and (9) into the system (4) and follow the algebraic procedure described in the Appendix to eliminate the z components of the electric and magnetic fields. As a result, the z components, E_z and H_z, turned out to be expressed in terms of the lateral components [see Eqs. (A5) and (A6)]. The resultant system of differential equations for the lateral components, $\mathbf{E}_P$ and $\mathbf{H}_P$, can be written in the following matrix form:

$$-i\,\partial_\tau\mathbf{F} = \widehat{\mathcal{M}} \cdot \mathbf{F} \equiv \begin{pmatrix} \widehat{\mathcal{M}}_{11} & \widehat{\mathcal{M}}_{12} \\ \widehat{\mathcal{M}}_{21} & \widehat{\mathcal{M}}_{22} \end{pmatrix} \begin{pmatrix} \mathbf{E}_P \\ \mathbf{H}_P \end{pmatrix}, \quad \tau = k_{\rm vac}z, \tag{10}$$

where the elements of the matrix differential operators $\widehat{\mathcal{M}}_{ij}$ are given by

$$\widehat{\mathcal{M}}^{(11)}_{\alpha\beta} = -\nabla_\alpha \cdot \left[\epsilon^{-1}_{zz}\epsilon_{z\beta}\right], \quad \widehat{\mathcal{M}}^{(12)}_{\alpha\beta} = \mu\delta_{\alpha\beta} - \nabla_\alpha \cdot \epsilon^{-1}_{zz} \cdot \nabla_\beta, \tag{11a}$$

$$\widehat{\mathcal{M}}^{(22)}_{\alpha\beta} = -\epsilon_{\alpha z}\epsilon^{-1}_{zz}\nabla_\beta, \quad \widehat{\mathcal{M}}^{(21)}_{\alpha\beta} = \epsilon^{(P)}_{\alpha\beta} - \mu^{-1}\nabla^{\perp}_\alpha \cdot \nabla^{\perp}_\beta, \tag{11b}$$

and the elements of the effective dielectric tensor (A8) that enter the operator $\widehat{\mathcal{M}}^{(21)}_{\alpha\beta}$ are

$$\epsilon^{(P)}_{\alpha\beta} = \epsilon_{\alpha\beta} - \epsilon_{\alpha z}\epsilon^{-1}_{zz}\epsilon_{z\beta}, \quad \alpha,\beta \in \{x,y\}. \tag{12}$$

B. Floquet harmonics

From Eq. (3), the dielectric tensor is a periodic function of x, so that it is represented by its Fourier series expansion

$$\varepsilon = \sum_{n=-\infty}^{\infty} \varepsilon_n \exp[in(\mathbf{k}_g \cdot \mathbf{r}_p)] = \sum_{n=-\infty}^{\infty} \varepsilon_n \exp(ink_g x), \tag{13}$$

where $\mathbf{r}_p \equiv (x,y,0)$. A similar representation applies to the coefficients that enter the differential operators (11).

The representation of Floquet harmonics [36] for solutions of the system (10),

$$\mathbf{F}(\mathbf{r}) = \mathbf{F}(\mathbf{r}_p,\tau) = \sum_{n=-\infty}^{\infty} \mathbf{F}_n(\tau)\exp\{i(\mathbf{k}_n \cdot \mathbf{r}_p)\},$$

$$\mathbf{k}_n = \mathbf{k}_p + n\mathbf{k}_g = k_{\rm vac}\mathbf{q}_n, \tag{14}$$

$$\mathbf{q}_n = q_n(\cos\phi_n\,\hat{\mathbf{x}} + \sin\phi_n\,\hat{\mathbf{y}}) = \left(q^{(n)}_x, q^{(n)}_y, 0\right), \tag{15}$$

where $\mathbf{k}_p$ is the tangential component of the wave vector of the incident plane wave defined in Eq. (7), is another consequence of the periodicity condition (3).

On substituting the expansion over the Floquet harmonics (14) into the system (10), we derive a set of matrix equations for the Floquet harmonics,

$$-i\,\partial_\tau \mathbf{F}_n(\tau) = \sum_{m=-\infty}^{\infty} \mathbf{M}_{nm}(\tau)\cdot\mathbf{F}_m(\tau), \tag{16}$$

$$\mathbf{M}_{nm} = \begin{pmatrix} \mathbf{M}^{(11)}_{nm} & \mathbf{M}^{(12)}_{nm} \\ \mathbf{M}^{(21)}_{nm} & \mathbf{M}^{(11)}_{nm} \end{pmatrix} = \frac{1}{\Lambda_g}\int_0^{\Lambda_g} \exp\{-i(\mathbf{k}_n\cdot\mathbf{r})\}[\widehat{\mathcal{M}}\exp\{i(\mathbf{k}_m\cdot\mathbf{r})\}]\mathrm{d}x, \tag{17}$$

where the 2×2 block matrices $\mathbf{M}^{(ij)}_{nm}$ are given by

$$\left[\mathbf{M}^{(11)}_{nm}\right]_{\alpha\beta} = -q^{(n)}_\alpha \beta^{(n-m)}_{z\beta}, \quad \left[\mathbf{M}^{(22)}_{nm}\right]_{\alpha\beta} = -\beta^{(n-m)}_{\alpha z} q^{(m)}_\beta, \tag{18a}$$

$$\left[\mathbf{M}^{(12)}_{nm}\right]_{\alpha\beta} = \mu\delta_{\alpha\beta}\delta_{nm} - q^{(n)}_\alpha\,\eta^{(n-m)}_{zz}\,q^{(m)}_\beta, \tag{18b}$$

$$\left[\mathbf{M}^{(21)}_{nm}\right]_{\alpha\beta} = \epsilon^{(n-m)}_{\alpha\beta} - \mu^{-1}\delta_{nm}\,p^{(n)}_\alpha p^{(m)}_\beta, \quad \mathbf{p}_n = \hat{\mathbf{z}}\times\mathbf{q}_n, \tag{18c}$$

and $\eta^{(n)}_{zz}$, $\beta^{(n)}_{ij}$, and $\epsilon^{(n)}_{\alpha\beta}$ are the Fourier coefficients for ϵ^{-1}_{zz}, $\epsilon^{-1}_{zz}\epsilon_{ij}$, and $\epsilon^{(P)}_{\alpha\beta}$, respectively.

General solution of the system (16),

$$\mathbf{F}_n(\tau) = \sum_{m=-\infty}^{\infty} \mathbf{U}_{nm}(\tau,\tau_0)\cdot\mathbf{F}_m(\tau_0), \tag{19}$$

can be conveniently expressed in terms of the *evolution operator* defined as the matrix solution of the initial value problem,

$$-i\,\partial_\tau \mathbf{U}_{nm}(\tau,\tau_0) = \sum_{k=-\infty}^{\infty} \mathbf{M}_{nk}(\tau)\cdot\mathbf{U}_{km}(\tau,\tau_0), \tag{20a}$$

$$\mathbf{U}_{nm}(\tau_0,\tau_0) = \mathbf{I}_4\,\delta_{nm}, \tag{20b}$$

where $\mathbf{I}_n$ is the $n\times n$ identity matrix.

The Floquet harmonics, $\mathbf{F}_n$, represent the electromagnetic field of the diffracted waves with the integer $n\in\mathbb{Z}$ giving the *diffraction order*. From the system (16), it can be inferred that the effect of interharmonics coupling responsible for diffraction is solely caused by the periodic modulation of the dielectric tensor (13).

In the ambient medium with $\epsilon_{ij} = \epsilon_{\rm m}\delta_{ij}$ and $\mu = \mu_{\rm m}$, the harmonics are decoupled and, for the nth diffraction order, represent plane waves propagating along the wave vectors with the tangential component (15). The Floquet harmonics of such waves, $\mathbf{F}^{(\rm m)}_n$, is given by

$$\mathbf{F}^{(\rm m)}_n(\tau) = \mathbf{V}_{\rm m}(\mathbf{q}_n)\begin{pmatrix} \exp\{i\mathbf{Q}_{\rm m}(q_n)\,\tau\} & \mathbf{0} \\ \mathbf{0} & \exp\{-i\mathbf{Q}_{\rm m}(q_n)\,\tau\}\end{pmatrix} \times \begin{pmatrix}\mathbf{E}^{(n)}_+ \\ \mathbf{E}^{(n)}_-\end{pmatrix}, \tag{21}$$

$$\mathbf{Q}_{\rm m}(q_n) = q_{\rm m}(q_n)\,\mathbf{I}_2, \quad q_{\rm m}(q_n) = \sqrt{n^2_{\rm m} - q^2_n}, \tag{22}$$

where $\mathbf{V}_{\rm m}(\mathbf{q}_n)$ is the eigenvector matrix for the ambient medium given by

$$\mathbf{V}_{\rm m}(\mathbf{q}_n) = \mathbf{T}_{\rm rot}(\phi_n)\mathbf{V}_{\rm m}(q_n) = \begin{pmatrix}\mathbf{R}_{\rm rot}(\phi_n) & \mathbf{0} \\ \mathbf{0} & \mathbf{R}_{\rm rot}(\phi_n)\end{pmatrix}\begin{pmatrix}\mathbf{E}_{\rm m} & -\boldsymbol{\sigma}_3\mathbf{E}_{\rm m} \\ \mathbf{H}_{\rm m} & \boldsymbol{\sigma}_3\mathbf{H}_{\rm m}\end{pmatrix}, \tag{23}$$

$$\mathbf{E}_{\rm m} = \begin{pmatrix} q_{\rm m}(q_n)/n_{\rm m} & 0 \\ 0 & 1\end{pmatrix}, \quad \mu_{\rm m}\,\mathbf{H}_{\rm m} = \begin{pmatrix} n_{\rm m} & 0 \\ 0 & q_{\rm m}(q_n)\end{pmatrix}, \tag{24}$$

$$\mathbf{R}_{\rm rot}(\phi) = \begin{pmatrix}\cos\phi & -\sin\phi \\ \sin\phi & \cos\phi\end{pmatrix}, \tag{25}$$

and $\{\boldsymbol{\sigma}_1,\boldsymbol{\sigma}_2,\boldsymbol{\sigma}_3\}$ are the Pauli matrices

$$\boldsymbol{\sigma}_1 = \begin{pmatrix}0 & 1\\ 1 & 0\end{pmatrix}, \quad \boldsymbol{\sigma}_2 = \begin{pmatrix}0 & -i\\ i & 0\end{pmatrix}, \quad \boldsymbol{\sigma}_3 = \begin{pmatrix}1 & 0\\ 0 & -1\end{pmatrix}. \tag{26}$$

From Eq. (21), the vector amplitudes $\mathbf{E}^{(n)}_+$ and $\mathbf{E}^{(n)}_-$ correspond to the forward and backward eigenwaves with $k^{(+)}_z = +k_{\rm vac}q_{\rm m}$ and $k^{(-)}_z = -k_{\rm vac}q_{\rm m}$, respectively. In the half space $z\leqslant 0$, these describe the *incident and reflected waves*,

$$\mathbf{E}^{(n)}_+|_{z\leqslant 0} = \mathbf{E}^{(n)}_{\rm inc} = \delta_{n\,0}\,\mathbf{E}_{\rm inc} \equiv \delta_{n\,0}\begin{pmatrix}E^{(\rm inc)}_p \\ E^{(\rm inc)}_s\end{pmatrix}, \tag{27}$$

$$\mathbf{E}^{(n)}_-|_{z\leqslant 0} = \mathbf{E}^{(n)}_{\rm refl} \equiv \begin{pmatrix}E^{(\rm refl)}_{p,\,n} \\ E^{(\rm refl)}_{s,\,n}\end{pmatrix}. \tag{28}$$

Clearly, Eq. (27) implies that the incident wave is the forward eigenwave of the zeroth order.

In the half space $z \geqslant D$ after the exit face of the grating, the only wave of the nth order is the *transmitted plane wave*:

$$\mathbf{E}_{+}^{(n)}|_{z\geqslant D} = \mathbf{E}_{\mathrm{trm}}^{(n)} \equiv \begin{pmatrix} E_{p,n}^{(\mathrm{trm})} \\ E_{s,n}^{(\mathrm{trm})} \end{pmatrix}, \quad \mathbf{E}_{-}^{(n)}|_{z\geqslant D} = \mathbf{0}. \tag{29}$$

Note that, at sufficiently large diffraction order with $q_n > n_{\mathrm{m}}$ and $q_{\mathrm{m}} = i|q_{\mathrm{m}}|$ [see Eq. (22)], the reflected and transmitted waves become evanescent. In this case, the z components of the wave vectors, $\mathbf{k}_{\mathrm{refl}}^{(n)} = k_{\mathrm{vac}}(-q_{\mathrm{m}}\,\hat{\mathbf{z}} + \mathbf{q}_n)$ and $\mathbf{k}_{\mathrm{trm}}^{(n)} = k_{\mathrm{vac}}(q_{\mathrm{m}}\,\hat{\mathbf{z}} + \mathbf{q}_n)$, are imaginary.

C. Computational procedure

We can now define the *transmission and reflection matrices* through the linear input-output relations

$$\mathbf{E}_{\mathrm{trm}}^{(n)} = \mathbf{T}_n \cdot \mathbf{E}_{\mathrm{inc}}, \quad \mathbf{E}_{\mathrm{refl}}^{(n)} = \mathbf{R}_n \cdot \mathbf{E}_{\mathrm{inc}}, \tag{30}$$

linking the nth order for the transmitted and reflected waves to the incident wave and, following the line of reasoning presented in Refs. [27,28], relate these matrices and the evolution operator given by Eq. (20). To this end, we use the boundary conditions requiring the tangential components of the electric and magnetic fields to be continuous at the boundary surfaces $\mathbf{F}_n(0) = \mathbf{F}_n^{(\mathrm{m})}(0-0)$ and $\mathbf{F}_n(h) = \mathbf{F}_n^{(\mathrm{m})}(h+0)$ and apply the relation (20) to the anisotropic layer of the thickness D to yield the following result:

$$\mathbf{F}_n^{(\mathrm{m})}(h+0) = \sum_k \mathbf{U}_{nk}(h,0) \cdot \mathbf{F}_k^{(\mathrm{m})}(0-0), \quad h = k_{\mathrm{vac}} D. \tag{31}$$

By using Eq. (21), Eq. (31) can be conveniently recast into the form

$$\begin{pmatrix} \mathbf{E}_{\mathrm{inc}}^{(n)} \\ \mathbf{E}_{\mathrm{refl}}^{(n)} \end{pmatrix} = \sum_k \mathbf{W}_{nk} \begin{pmatrix} \mathbf{E}_{\mathrm{trm}}^{(k)} \\ \mathbf{0} \end{pmatrix}, \tag{32}$$

where $\mathbf{W}_{nk}$ is given by

$$\mathbf{W}_{nk} = [\mathbf{V}_{\mathrm{m}}(\mathbf{q}_n)]^{-1} \cdot [\mathbf{U}^{-1}(h,0)]_{nk} \cdot \mathbf{V}_{\mathrm{m}}(\mathbf{q}_k) = \begin{pmatrix} \mathbf{W}_{nk}^{(11)} & \mathbf{W}_{nk}^{(12)} \\ \mathbf{W}_{nk}^{(21)} & \mathbf{W}_{nk}^{(22)} \end{pmatrix} \tag{33}$$

and defines the so-called *linking matrix*.

At $n \neq 0$, the relation (32) gives the system for the transmitted wave orders

$$-\mathbf{W}_{n0}^{(11)} \cdot \mathbf{E}_{\mathrm{trm}}^{(0)} = \sum_{k\neq 0} \mathbf{W}_{nk}^{(11)} \cdot \mathbf{E}_{\mathrm{trm}}^{(k)}, \quad n \neq 0. \tag{34}$$

By solving this system we obtain the diffracted waves

$$\mathbf{E}_{\mathrm{trm}}^{(n)} = \tilde{\mathbf{T}}_n \cdot \mathbf{E}_{\mathrm{trm}}^{(0)} \tag{35}$$

linearly related to the zeroth order (nondiffracted wave) through the efficiency matrices $\tilde{\mathbf{T}}_n$. Obviously, Eq. (35) implies that, by definition, $\tilde{\mathbf{T}}_0 = \mathbf{I}_2$.

From Eq. (32) at $n = 0$, we derive the relation

$$\mathbf{E}_{\mathrm{inc}} = \sum_k \mathbf{W}_{0k}^{(11)} \cdot \mathbf{E}_{\mathrm{trm}}^{(k)}, \tag{36}$$

linking the vector amplitudes of the incident and transmitted waves. Substitution of the matrices from Eq. (35) into Eq. (36) provides the transmission matrix (30) in the following form:

$$\mathbf{T}_n = \tilde{\mathbf{T}}_n \cdot \left[\sum_k \mathbf{W}_{0k}^{(11)} \cdot \tilde{\mathbf{T}}_k\right]^{-1}. \tag{37}$$

From the relation (32) applied to the case of reflected waves, we derive the reflection matrix

$$\mathbf{R}_n = \sum_k \mathbf{W}_{nk}^{(21)} \cdot \mathbf{T}_k \tag{38}$$

expressed in terms of the transmission matrices (37).

In the limiting case of uncoupled harmonics, where $\mathbf{W}_{nk} = \delta_{nk}\mathbf{W}_{nn}$, it is not difficult to recover the results for stratified media obtained in Refs. [27,28]. It suffices to note that, at $\mathbf{W}_{0n}^{(11)} = \mathbf{0}$, the system (34) gives the efficiency matrices $\tilde{\mathbf{T}}_n = \delta_{n0}\,\mathbf{I}_2$ indicative of the absence of diffracted waves.

III. DEFORMED HELIX FERROELECTRIC LIQUID CRYSTAL CELLS

In this section we present the experimental results on the transmittance of light passing through crossed polarizers measured as a function of the applied electric field in DHFLC cells. In order to interpret the experimental data, the theoretical approach of Sec. II is applied to chiral smectic helical configurations with the subwavelength helix pitch.

A. Experiment

1. Material and sample preparation

In our experiments we used the FLC mixture FLC-576A (from P. N. Lebedev Physical Institute of Russian Academy of Sciences) as a material for the DHFLC layer. Following the procedure described in Ref. [37], we have measured the temperature dependence of the helix pitch shown in Fig. 3. It can be seen that, at room temperature, this mixture has the helix pitch, P, around 200 nm.

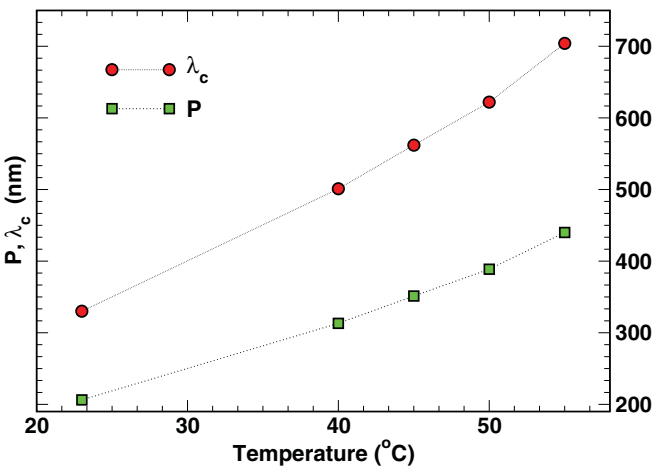

FIG. 3. (Color online) Maximum selective reflection wavelength, λ_c, measured as a function of temperature and the FLC helix pitch evaluated from the formula $P = 2\lambda_c/(n_o + n_e)$.

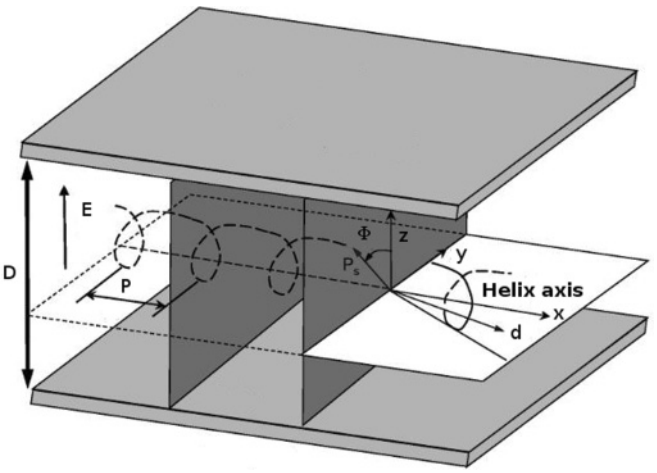

FIG. 4. Geometry of a DHFLC cell of thickness D. The applied electric field, **E**, is normal to both the substrates and the FLC helix axis.

Hence, in the visible spectral range, the light scattering turns out to be completely suppressed [37], except that the applied voltage is close to the critical voltage of the helix unwinding. So, such mixtures exhibit pronounced effects of electrically controlled phase retardation and birefringence $\Delta n_{\text{eff}}(E)$ that can be clearly detected.

The photoalignment technique described in Refs. [38,39] was used for producing the FLC cells. Following the method of Ref. [38], indium tin oxide (ITO) surfaces of FLC cells were covered with a 10-to-20-nm photoaligning substance, azobenzene sulfonic dye SD-1 layers. The azo-dye solution was spin coated onto an ITO electrode and dried at 155 °C.

The surface of the coated film was illuminated with linearly polarized UV light using a super-high-pressure Hg lamp through an interference filter at the wavelength 365 nm and a polarizing filter. The intensity of light irradiated normally on the film surface during 30 min was 6 mW/cm^2.

The geometry of the cells is schematically depicted in Fig. 4. We used the cells with the size of 13×13 mm^2, the thickness of the glass substrate 1.1 mm, electrode area 10×10 mm^2, and the cell thickness (gap) 52 and 130 μm. The FLC mixture was injected into the cells in the isotropic phase by capillary action. As in Ref. [40], in order to obtain a nearly defectless DHF structure, the cells were subjected to an alternate electrical training.

2. *Experimental setup*

The measurements of the light transmittance in relation to the applied voltage were performed at wavelength $\lambda = 650$ nm in the automatic regime. For this purpose, the measurement complex device was built whose principal scheme is shown in Fig. 5. The basic element of this experimental setup is computer data acquisition (DAQ) board NIPCI 6251 from National Instruments. This board has two analog outputs and 16 analog inputs. The operating voltage is ± 10 V and the maximal registration speed is 1 μs. The board has independent output and input buffers for 4000 points. In our experiments, the output signal, 10 V, was not sufficient and the wideband power amplifier KH model 7600 from Krohn-Hite Corporation

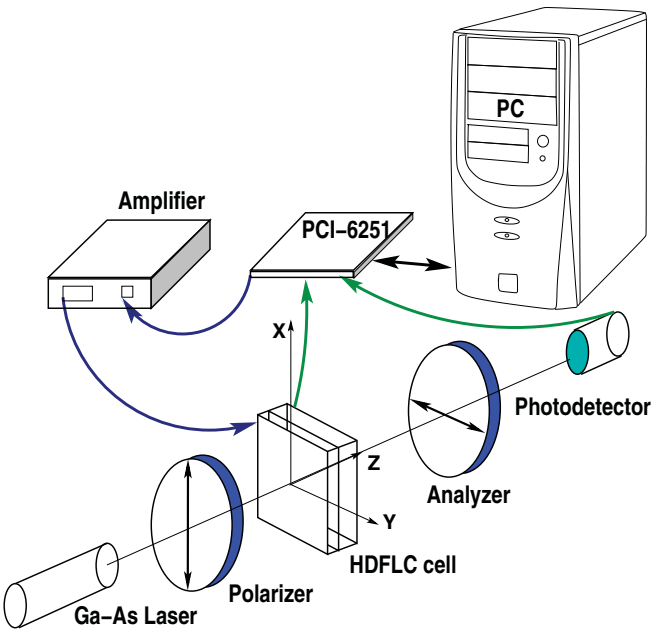

FIG. 5. (Color online) Experimental setup for electro-optical measurements of DHFLC cells. A cell placed between crossed polarizers is illuminated with light from a semiconductor Ga-As laser ($\lambda = 650$ nm) and the output is collected by a photodetector.

with amplification coefficients 5 and 25 times was used. It gives a possibility to have the output signal up to ± 250 V. For the input signal this board has an internal amplifier with coefficients 1, 2, 4, 8, 16, 32, 64, and 128 times. A photodetector was connected to input board plate for optical measurements.

The software for experimental setup has built-in functions for analog output-input. The program has three functional blocks that make operations with the setup highly effective. The first block is a programmable generator capable of producing any form of signal with a duration of 2000 points. The duration of one point can be set from 1 μs to 1 s. The second block is a measuring block, which saves 4000 values of the input voltage with step from 1 μs to 1 s. The operation of the first and the second blocks is synchronized inside the DAQ board and cannot be disturbed by computer interruptions. The third block is used to accumulate the experimental data during the working period.

B. Theory

In this section we apply our general theoretical approach described in Sec. II to the special case of DHFLC PGs. As is schematically shown in Figs. 1 and 4, in DHFLCs, the director

$$\hat{\mathbf{d}} = (d_x, d_y, d_z) = \cos\theta_t\, \hat{\mathbf{x}} + \sin\theta_t\, \cos\Phi\, \hat{\mathbf{y}} + \sin\theta_t\, \sin\Phi\, \hat{\mathbf{z}} \tag{39}$$

lies on the smectic cone with the *smectic tilt angle* θ_t and rotates in a helical fashion about a uniform in-plane twist axis (the x axis) forming the FLC helix.

In the presence of weak electric field, $\mathbf{E} = E\,\hat{\mathbf{z}}$, which is well below its critical value at the helix unwinding transition,

$E \ll E_c$, the azimuthal angle around the cone, Φ, can be written in the form [30,32,35]

$$\Phi = \phi + \Delta\Phi(\phi) \approx \phi + \alpha_E \sin\phi, \quad \phi = \frac{2\pi}{P}\, x, \quad (40)$$

where the electric field induced distortion $\Delta\Phi$ linearly depends on E through the *electric field parameter* α_E proportional to the ratio of the applied and critical electric fields: E/E_c.

From Eq. (40), it is clear that in the regime of a weak electric field, the *helix pitch* P defines both the grating period, $\Lambda_g = P$, and the grating wave number, $k_g = 2\pi/P$. For the LC dielectric tensor (1) with the DHF helical configuration (39), the anisotropy parameters that enter the matrices $\mathbf{M}_{mn}$ whose block structure is described in Eq. (18) are given by

$$\epsilon_\perp \eta_{zz} = \frac{1}{1 + u_a d_z^2} = \frac{1}{1 + v\sin^2\Phi}, \quad v = u_a \sin^2\theta_t, \quad (41)$$

$$\beta_{\alpha z} = \beta_{z\alpha} = \frac{u_a d_z d_\alpha}{1 + v\sin^2\Phi}, \quad (42)$$

$$\epsilon_\perp^{-1}\epsilon_{\alpha\beta}^{(P)} = \delta_{\alpha\beta} + \frac{u_a d_\alpha d_\beta}{1 + v\sin^2\Phi}. \quad (43)$$

According to the computational procedure developed in the previous section, after inserting the above parameters into the matrices of the system (16) for the Floquet harmonics, we need to find the evolution operator by solving the initial value problem (20). Then computing the transmission and the reflection matrices (30) involve the following steps: (a) evaluation of the linking matrix (33); (b) calculation of the efficiency matrices (35) by solving the system of linear equation (34); (c) computing the matrices $\mathbf{T}_n$ and $\mathbf{R}_n$ from the formulas (37) and (38), respectively.

As a consequence of the anisotropy induced mode coupling, there are an infinite number of coupled matrix equations in the system (16). So the evolution operator cannot be generally computed in the closed form without resorting to the methods of the perturbation theory or numerical analysis.

In this paper, we restrict ourselves to the case where the helix pitch is smaller than the wavelength, $P < \lambda$, so as to interpret the experimental data measured in DHFLC cells with the subwavelength pitch. In our experiments, the incident light travels in the air with and normally impinges on the cell. At $n_\mathrm{m} = 1$ and $k_p = 0$, the condition

$$q_g \equiv k_g/k_\mathrm{vac} = \lambda/P > 1 \quad (44)$$

implies that $q_n > n_\mathrm{m}$. In this case, from the above discussion after Eq. (29), there are no diffracted waves propagating in the air and nonzero orders of the transmitted and reflected beams are evanescent. In the zero-order approximation, where $\mathbf{M}_{mn} = \delta_{m0}\delta_{n0}\mathbf{M}_{00}$, the evanescent waves are neglected and the DHFLC cell appears to be effectively described as a uniformly anisotropic layer characterized by the matrix

$$\mathbf{M}_{00} \equiv \langle\mathbf{M}\rangle = \begin{pmatrix} \langle\mathbf{M}\rangle_{11} & \langle\mathbf{M}\rangle_{12} \\ \langle\mathbf{M}\rangle_{21} & \langle\mathbf{M}\rangle_{22} \end{pmatrix}, \quad (45)$$

where $\langle\cdots\rangle = (2\pi)^{-1}\int_o^{2\pi}\cdots \mathrm{d}\phi$. The elements of the 2×2 block matrices $\langle\mathbf{M}\rangle_{ij}$ are given by

$$\langle\mathbf{M}\rangle_{\alpha\beta}^{(11)} = -q_\alpha^{(p)}\langle\beta_{z\beta}\rangle, \quad \langle\mathbf{M}\rangle_{\alpha\beta}^{(22)} = -\langle\beta_{\alpha z}\rangle q_\beta^{(p)}, \quad (46)$$

$$\langle\mathbf{M}\rangle_{\alpha\beta}^{(12)} = \mu\delta_{\alpha\beta} - q_\alpha^{(p)}\langle\eta_{zz}\rangle\, q_\beta^{(p)}, \quad (47)$$

$$\langle\mathbf{M}\rangle_{\alpha\beta}^{(21)} = \epsilon_{\alpha\beta}^{(\mathrm{eff})} - \mu^{-1}\, p_\alpha^{(p)} p_\beta^{(p)}, \quad \mathbf{p}_p = \hat{\mathbf{z}}\times\mathbf{q}_p, \quad (48)$$

where $k_\mathrm{vac}\mathbf{q}_p = \mathbf{k}_p$ and $\epsilon_{\alpha\beta}^{(\mathrm{eff})} = \langle\epsilon_{\alpha\beta}^{(P)}\rangle$ is the averaged effective dielectric tensor.

1. Effective dielectric tensor

Our next step is to evaluate the averages that enter the matrix (45). We note that, from Eq. (42) and the result

$$\langle\sin\Phi\,[1 + v\sin^2\Phi]^{-1}\rangle = 0 = \langle\sin\Phi\cos\Phi\,[1 + v\sin^2\Phi]^{-1}\rangle, \quad (49)$$

the averages $\langle\beta_{\alpha z}\rangle$ are zero. When the averaged matrix (45) at $\langle\beta_{\alpha z}\rangle = 0$ is compared with the matrix of a uniformly anisotropic layer (see, e.g., Eq. (25) in Ref. [28]), where $\langle\beta_{\alpha z}\rangle = \epsilon_{\alpha z}/\epsilon_{zz}$, $\langle\eta_{zz}\rangle = 1/\epsilon_{zz}$ and $\epsilon_{\alpha\beta}^{(\mathrm{eff})} = \epsilon_{\alpha\beta}^{(P)}$, it immediately follows that the effective anisotropic medium is biaxial. In this medium, the diagonal element

$$\epsilon_{zz}^{(\mathrm{eff})} = n_z^2/\mu = \langle\eta_{zz}\rangle^{-1} \quad (50)$$

gives the principal value of the effective dielectric tensor for the optic axis normal to the cell (parallel to the z axis).

For our purposes, it suffices to expand the averages up to second-order terms in the field parameter,

$$\langle[1 + v\sin^2\Phi]^{-1}\rangle \approx [1+v]^{-1/2}\big(1 + v\gamma_v^2\alpha_E^2\big), \quad (51)$$

$$\langle\cos^2\Phi\,[1 + v\sin^2\Phi]^{-1}\rangle \approx \gamma_v\big(1 + [1+v]^{1/2}\gamma_v\alpha_E^2\big), \quad (52)$$

$$\langle\cos\Phi\,[1 + v\sin^2\Phi]^{-1}\rangle \approx -\gamma_v\alpha_E, \quad \gamma_v \equiv (\sqrt{1+v} - 1)/v, \quad (53)$$

so that the in-plane components of the dielectric tensor are given by

$$\epsilon_{xy}^{(\mathrm{eff})} = \gamma_{xy}\alpha_E, \quad \gamma_{xy} = -\cos\theta_t\sin\theta_t\gamma_v(\epsilon_\parallel - \epsilon_\perp), \quad (54a)$$

$$\epsilon_{xx}^{(\mathrm{eff})} = \bar{\epsilon} + \Delta\epsilon = \epsilon_{xx}^{(0)} + \gamma_{xx}\alpha_E^2, \quad (54b)$$

$$\epsilon_{yy}^{(\mathrm{eff})} = \bar{\epsilon} - \Delta\epsilon = \epsilon_{yy}^{(0)} + \gamma_{yy}\alpha_E^2, \quad (54c)$$

where

$$\epsilon_{xx}^{(0)} = \epsilon_\perp(1 + (u_a - v)[1+v]^{-1/2}), \quad \epsilon_{yy}^{(0)} = \epsilon_\perp[1+v]^{-1/2}, \quad (55)$$

$$\gamma_{xx} = \epsilon_\perp(u_a - v)v[1+v]^{-1/2}\gamma_v^2, \quad \gamma_{yy} = \epsilon_\perp v[1+v]^{1/2}\gamma_v^2. \quad (56)$$

Similar to the LC dielectric tensor (1), the tensor (54) can be expressed in terms of the "director" (the in-plane optical axis) $\hat{\mathbf{d}}_\mathrm{eff} = (d_x^{(\mathrm{eff})}, d_y^{(\mathrm{eff})}, 0) = (\cos\phi_\mathrm{d}, \sin\phi_\mathrm{d}, 0)$ with the azimuthal angle, ϕ_d, defined by the relation

$$\tan(2\phi_\mathrm{d}) = \gamma_{xy}\alpha_E/\Delta\epsilon \quad (57)$$

and its eigenvalues

$$\epsilon_\pm = n_\pm^2/\mu = \bar{\epsilon} \pm \Delta\epsilon\sqrt{1 + \tan^2(2\phi_\mathrm{d})} \quad (58)$$

as follows:

$$\epsilon_{\alpha\beta}^{(\mathrm{eff})} = \epsilon_-\delta_{\alpha\beta} + (\epsilon_+ - \epsilon_-)d_\alpha^{(\mathrm{eff})}d_\beta^{(\mathrm{eff})}. \quad (59)$$

2. Light transmittance

In the case of normal incidence, the transmission and reflection matrices can be easily obtained from the results of Refs. [41,42] in the limit of the wave vectors with vanishing tangential component, $k_p = 0$. For our purposes, we need to write the resultant expression for the transmission matrix as

$$\mathbf{T}(\phi_{\rm d}) \equiv \begin{pmatrix} t_{xx} & t_{xy} \\ t_{yx} & t_{yy} \end{pmatrix} = \frac{t_+ + t_-}{2}\,\mathbf{I}_2 + \frac{t_+ - t_-}{2}\,\mathbf{R}_{\rm rot}(2\phi_{\rm d})\cdot\boldsymbol{\sigma}_3, \tag{60}$$

$$t_\pm = \frac{1-\rho_\pm^2}{1-\rho_\pm^2\exp(2in_\pm h)}\exp(in_\pm h),$$
$$\rho_\pm = \frac{n_\pm/\mu - n_{\rm m}/\mu_{\rm m}}{n_\pm/\mu + n_{\rm m}/\mu_{\rm m}}. \tag{61}$$

When the incident wave is linearly polarized along the x axis (the helix axis), the transmittance coefficient

$$T_{xy} = |t_{xy}|^2 = \frac{|t_+ - t_-|^2}{4}\,\sin^2(2\phi_{\rm d}),$$
$$\sin^2(2\phi_{\rm d}) = \frac{\alpha_E^2}{\alpha_E^2 + (\Delta\epsilon/\gamma_{xy})^2}, \tag{62}$$

where $h = k_{\rm vac}D$ is the thickness parameter, describes the intensity of the light passing through crossed polarizers. Note that, under certain conditions such as $|\rho_\pm| \ll 1$, $t_\pm \approx \exp(in_\pm h)$ and the transmittance (62) can be approximated by the simpler formula

$$T_{xy} \approx \sin^2(\delta/2)\,\sin^2(2\phi_{\rm d}), \tag{63}$$

where $\delta = \Delta n_{\rm eff}\,h = (n_+ - n_-)h$ is the difference in optical path of the ordinary and extraordinary waves known as the *phase retardation*.

In the general case when the incident light is elliptically polarized with the circular components,

$$E_\pm^{(\rm inc)} \propto \exp\left[\mp i\phi_p^{(\rm inc)}\right]\left(1 \pm \epsilon_{\rm ell}^{(\rm inc)}\right) \tag{64}$$

expressed in terms of the polarization azimuth, $\phi_p^{(\rm inc)}$, and the ellipticity, $\epsilon_{\rm ell}^{(\rm inc)}$, the expression (60) gives the components of the transmitted wave that can be written in the following form:

$$2\exp\left[\pm i\phi_p^{(\rm inc)}\right]E_\pm^{(\rm trm)} = (t_+ + t_-)\left(1 \pm \epsilon_{\rm ell}^{(\rm inc)}\right)$$
$$+\exp\left[\mp 2i\left(\phi_{\rm d} - \phi_p^{(\rm inc)}\right)\right](t_+ - t_-)\left(1 \mp \epsilon_{\rm ell}^{(\rm inc)}\right), \tag{65}$$

where $E_\pm^{(\alpha)} = (E_x^{(\alpha)} \mp i\,E_y^{(\alpha)})/\sqrt{2}$.

C. Experimental results and modeling

Now we turn back to the electro-optical measurements in the DHFLC cells described in Sec. III A. The transmittance versus electric field curve shown in Fig. 6 presents the results measured at the wavelength of light generated by the Ga-As laser with $\lambda = 650$ nm in the cell in which the thickness of the DHFLC layer, D, was about 130 μm.

The formula for the transmittance (62) can be combined with the expressions for the principal values of the effective refractive indices (58) to evaluate dependence of T_{xy} on the applied electric field, E. The known parameters characterizing the FLC mixture FLC-576A that enter our formulas are the ordinary (extraordinary) refractive index and the tilt angle estimated at $n_o = 1.5$ ($n_e = 1.72$) and $\theta_t = 32^\circ$, respectively. So, for the anisotropy parameters, u_a and v, we have $u_a \approx 0.315$ and $v = u_a \sin^2\theta_t \approx 0.09$.

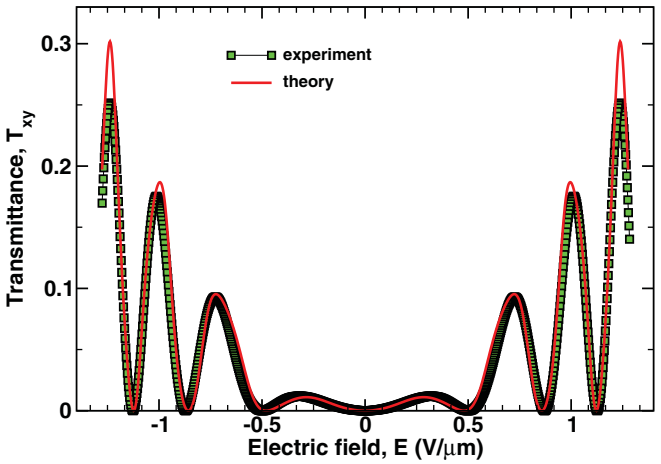

FIG. 6. (Color online) Transmittance of light passing through crossed polarizers, T_{xy}, as a function of the applied electric field for the DHFLC cell of thickness $D = 130$ μm filled with the FLC mixture FLC-576A. Parameters of the mixture are as follows: $n_o = 1.5$ ($n_e = 1.72$) is the ordinary (extraordinary) refractive index and $\theta_t = 32^\circ$ is the tilt angle. The experimental points are marked by squares. The solid line represents the theoretical curve computed for the electric field parameter $\alpha_E = \gamma_E E$ with $\gamma_E \approx 0.64$ μm/V.

From the discussion after Eq. (40), the electric field parameter α_E is proportional to the electric field, $\alpha_E = \gamma_E E$, and thus is determined by the coefficient of proportionality γ_E. This coefficient is the sole fitting parameter in our calculations.

Figure 6 shows that, when the cell thickness is 130 μm, the theoretical curve computed at $\gamma_E \approx 0.64$ μm/V and the experimental data are in close agreement. Similarly, in Fig. 7, the transmittance T_{xy} is plotted against the applied electric field, E, for the case where the cell thickness is about 52 μm.

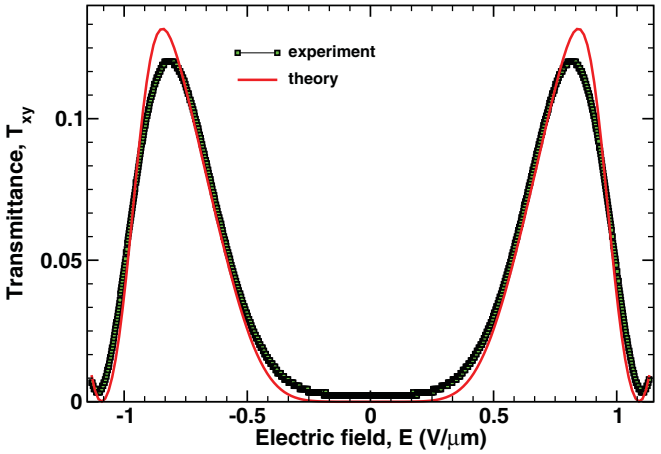

FIG. 7. (Color online) Light transmittance, T_{xy}, of the DHFLC cell versus applied electric field, E. The cell is filled with the FLC mixture FLC-576A and its thickness is estimated at about $D = 52$ μm so that $\sin[\delta(0)/2] \approx 0$. The experimental points are marked by squares. The theoretical curve (solid line) is computed at $\alpha_E = \gamma_E E$ and $\gamma_E \approx 0.64$ μm/V.

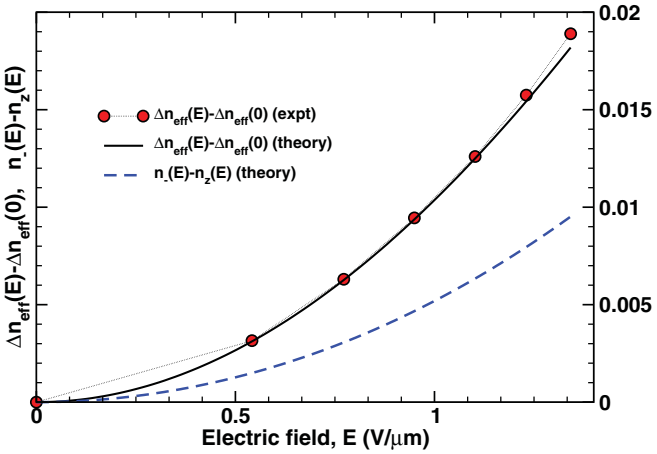

FIG. 8. (Color online) Electrically controlled birefringence, $\Delta n_{\rm eff}(E) - \Delta n_{\rm eff}(0)$, and refractive index difference, $n_-(E) - n_z(E)$, as a function of electric field. The theoretical curves (solid and dashed lines) are computed from Eqs. (58) and (41), respectively, at $\alpha_E = \gamma_E E$ with $\gamma_E \approx 0.64\ \mu$m/V.

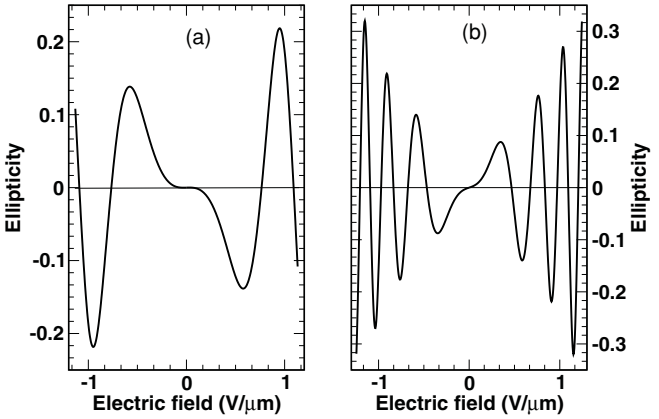

FIG. 9. Electric field dependence of transmitted light ellipticity for the two DHFLC cells with (a) $D = 52\ \mu$m and (b) $D = 130\ \mu$m. The curves are computed at $\phi_p^{(\rm inc)} = 0$ and $\epsilon_{\rm ell}^{(\rm inc)} = 0$ (linearly polarized incident light).

Referring to Figs. 6 and 7, the transmittance oscillates with the magnitude of the applied field. From Eqs. (61) and (62), this is the dependence of the effective refractive indices, n_+ and n_-, on the electric field parameter, α_E, that manifests itself in these oscillations. More precisely, as is evident from the approximate expression for the transmittance (63), they are due to variations in the phase retardation, δ, arising from the electric field induced birefringence, $\Delta n_{\rm eff} = n_+ - n_-$. So, loci of extrema (minima and maxima) of the transmittance, T_{xy}, can be used to obtain dependence of the birefringence on the applied electric field (more details on this method can be found, for example, in Refs. [40,43]).

Figure 8 shows the results for the field dependence of the electrically controlled birefringence, $\Delta n_{\rm eff}(E) - \Delta n_{\rm eff}(0)$, measured for the mixture FLC-576A. As can be seen from the figure, there is a remarkable accord between the experimental points and the curve evaluated from the principal values (58) of the effective dielectric tensor (59). From Eq. (58), it follows that, when the electric field parameter, α_E, is sufficiently small, the principal refractive indices n_+ and n_- exhibit the Kerr-like quadratic nonlinearity: $n_\pm(E) - n_\pm(0) \propto E^2$. A similar representation applies to the refractive index difference $n_-(E) - n_z(E)$ characterizing biaxiality. Referring to Fig. 8, the electrically controlled birefringence is nearly twice as much as the biaxility difference, $n_- - n_z$.

In addition to the birefringence, the transmittance (62) depends on the azimuthal angle, $\phi_{\rm d}$, given in Eq. (57). This angle describes the electric field induced rotation of the optical axes of the dielectric tensor (59) and, under the action of the electric field, E, its magnitude varies in the range between zero and $\pi/4$.

A quick inspection of the formula (62) shows that the transmittance will always vanish in the zero-field limit with $E = 0$, so that $\phi_{\rm d} \propto E$ at small E [see also Eq. (57)]. Such behavior, however, comes as no surprise if we recall that the electric field of the incident wave is assumed to be parallel to the helix axis, $\mathbf{E}_{\rm inc} \parallel \hat{\mathbf{x}}$, which is the zero-voltage optical axis.

Interestingly, the transmittance versus electric field curve will flatten in the vicinity of the origin when the cell thickness is chosen in such way that, in addition to $\sin\phi_{\rm d}$, the birefringence dependent factor equals zero at $E = 0$. The latter is the case for the curves shown in Fig. 7, where $\sin\delta(0)/2 \approx 0$ at $D \approx 52\ \mu$m.

So, we have found that the value of the sole fitting parameter γ_E is about 0.64 μm/V. This value has been used to estimate effective biaxiality by computing the refractive index difference, $n_- - n_z$, as a function of electric field (see Fig. 8). As another prediction of the theory, the ellipticity of transmitted light is plotted against the electric field in Fig. 9. Note that this dependence is calculated from the formula (65) and can, in principle, be tested experimentally. Additional experimental studies dealing with the effects of biaxiality and ellipticity are under progress and the results will be presented elsewhere.

IV. DISCUSSION AND CONCLUSIONS

In this paper we have formulated the theoretical approach to the optical properties of PGs that can be regarded as an extension of the method developed in Refs. [27,28] for stratified anisotropic media. Mathematically, in this approach, the key formulas (37) and (38) give the transmission and reflection matrices of diffraction orders, $\mathbf{T}_n$ and $\mathbf{R}_n$, expressed in terms of the linking matrix (33) which is related to the evolution operator (20) of the system of matrix equations (16) for the Floquet harmonics (14) derived from the Maxwell's equations for the lateral components of the electric and magnetic fields (10).

This method goes beyond the well-known limitations of the Jones matrix formalism at the expense of simplicity. To some extent it can be regarded as a version of the coupled mode analysis and our derivation of equations for the Floquet harmonics bear some similarity to the differential theory of light diffraction [44], which is based on the integration of a differential set of equations derived from Maxwell's equations projected onto some functional bases. In particular, as was pointed out in Refs. [45,46], this theory can be applied to the

special case of crossed anisotropic gratings that were analyzed by using the Fourier modal method in Ref. [46].

In contrast to a theoretical method recently suggested in [47] for a reverse twisted nematic LC grating, our approach is formulated without recourse to the vector theory of scattering for a far field. It also does not rely on the assumptions behind averaging procedure for the transmittance used in Ref. [48].

Note that the optical properties of PGs were also analyzed numerically using the finite-difference time-domain method in Ref. [49]. Although such analysis is general and useful, it can be very computationally intense so as to produce the results of sufficiently high accuracy.

We have used the method described in Sec. II as a tool of theoretical investigation into the electro-optical properties of DHFLC gratings with subwavelength pitch. It was previously demonstrated that a short helix pitch FLC ($P = 0.4$–$0.8\ \mu$m) provides an effective phase shift change of a transmitted polarized light beam as a function of the applied electric field intensity [29]. The new mixtures with the helix pitch being in UV region [37] make it possible to get rid of complications related to the light scattering effects.

So, in such mixtures, we deal with a pure electrically controlled phase shift plate based on the electro-optical mode called DHF. DHF is a convenient operation mode able to ensure both low voltage and fast switching liquid crystalline light shutters (the response time is less than 100 μs at driving electric field around 1 V/μm). For these reasons, it is important to understand the behavior of the electrically controlled birefringence in such DHFLC cells.

We have shown that, in the short-pitch approximation, DHFLC cells are equivalent to uniformly anisotropic biaxial layers with the optical axis normal to the substrate plane. The latter implies that normally incident light feels only uniaxial in-plane anisotropy in agreement with the recent results on the ellipticity of light transmitted through a DHFLC cell [40].

We have computed the averaged dielectric tensor as a function of the applied electric field and have used the results to evaluate the light transmittance measured in our experiments. A comparison between theoretical and experimental results presented in Figs. 6–8 shows that the predictions of the theory are in good agreement with the experimental data.

Note that our calculations of the averaged dielectric tensor rely on the approximate expression for the azimuthal angle (40) which is applicable for sufficiently low voltages. A more accurate description of the DHFLC orientational structure is required when the voltage increases approaching the unwinding transition [50].

ACKNOWLEDGMENTS

This work is supported by HKUST Grants No. CERG 612208, No. CERG 612310, and No. CERG 612409. A.D.K acknowledges partial financial support under STCU Grant No. 4687 and is grateful to Nelson Tabiryan for stimulating remarks. E.P.P. was also supported by Russian Foundation of Basic Research (RFBR) Grants No. 09-03-12234-ofi-m, No. 09-03-12263-ofi-m, No. 10-02-01336-a, No. 10-03-13305-omi, No. 10-03-90016-Bel-a, No. 08-02-01074-a and by the Russian Federal Agency of Science and Innovations (Project No. 02.740.11.5166).

APPENDIX: DERIVATION OF EQUATIONS FOR LATERAL COMPONENTS

In this section we discuss how to exclude the z components of the electromagnetic field, E_z and H_z, that enter the representation (8) from the Maxwell equations (4). Our task is to derive the closed system of equations for the lateral (tangential) components, $\mathbf{E}_P$ and $\mathbf{H}_P$.

We begin with substituting Eqs. (8) and (9) and have Maxwell's equations (4) recast into the form

$$-i\partial_\tau\,[\hat{\mathbf{z}}\times\mathbf{E}_P] = \mu\mathbf{H} - \nabla_p\times\mathbf{E}, \tag{A1a}$$

$$-i\partial_\tau\,\mathbf{H}_P = \mathbf{D} + \nabla_p\times\mathbf{H}, \tag{A1b}$$

where the explicit expressions for the last terms on the right-hand side of the system (A1) are as follows:

$$\nabla_p\times\mathbf{E} = -\nabla_p^\perp E_z + (\nabla_p^\perp\cdot\mathbf{E}_P)\,\hat{\mathbf{z}}, \tag{A2a}$$

$$\nabla_p\times\mathbf{H} = -\nabla_p^\perp H_z + (\nabla_p\cdot\mathbf{H}_P)\,\hat{\mathbf{z}}. \tag{A2b}$$

We can now substitute the electric displacement field written as a sum of the normal and in-plane components,

$$\mathbf{D} = D_z\hat{\mathbf{z}} + \mathbf{D}_P, \tag{A3}$$

into Eq. (A1b) and derive the following expression for its z component:

$$D_z = \epsilon_{zz}E_z + (\boldsymbol{\epsilon}_z\cdot\mathbf{E}_P) = -(\nabla_p\cdot\mathbf{H}_P), \tag{A4}$$

where $\boldsymbol{\epsilon}_z = (\epsilon_{zx},\epsilon_{zy})$.

From Eqs. (A1) and (A4), it is not difficult to deduce the relations

$$H_z = \mu^{-1}(\nabla_p^\perp\cdot\mathbf{E}_P), \tag{A5}$$

$$E_z = -\epsilon_{zz}^{-1}[(\boldsymbol{\epsilon}_z\cdot\mathbf{E}_P) + (\nabla_p\cdot\mathbf{H}_P)], \tag{A6}$$

linking the normal (along the z axis) and the lateral (perpendicular to the z axis) components.

By using the relation (A6), we obtain the tangential component of the field (A3),

$$\mathbf{D}_P = \boldsymbol{\epsilon}_z' E_z + \boldsymbol{\varepsilon}_z\cdot\mathbf{E}_P = \boldsymbol{\varepsilon}_P\cdot\mathbf{E}_P - \boldsymbol{\epsilon}_z'\epsilon_{zz}^{-1}(\nabla_p\cdot\mathbf{H}_P), \tag{A7}$$

where

$$\boldsymbol{\varepsilon}_z = \begin{pmatrix}\epsilon_{xx} & \epsilon_{xy}\\ \epsilon_{yx} & \epsilon_{yy}\end{pmatrix};$$

$\boldsymbol{\epsilon}_z' = (\epsilon_{xz},\epsilon_{yz})$ and the effective dielectric tensor, $\boldsymbol{\varepsilon}_P$, for the lateral components is given by

$$\boldsymbol{\varepsilon}_P = \varepsilon_z - \epsilon_{zz}^{-1}\,\boldsymbol{\epsilon}_z'\otimes\boldsymbol{\epsilon}_z. \tag{A8}$$

Maxwell's equations (A1) can now be combined with the relations (A2) to yield the system

$$-i\partial_\tau\,\mathbf{E}_P = \mu\mathbf{H}_P + \nabla_p E_z, \tag{A9a}$$

$$-i\partial_\tau\,\mathbf{H}_P = \mathbf{D}_P - \nabla_p^\perp H_z, \tag{A9b}$$

where H_z, E_z, and $\mathbf{D}_P$ are given in Eq. (A5), Eq. (A6), and Eq. (A7), respectively.

So, this system immediately gives the final result

$$-i\partial_\tau \mathbf{E}_P = -\nabla_p\left[\epsilon_{zz}^{-1}(\boldsymbol{\epsilon}_z \cdot \mathbf{E}_P)\right] + \mu \mathbf{H}_P - \nabla_p\left[\epsilon_{zz}^{-1}(\nabla_p \cdot \mathbf{H}_P)\right], \quad \text{(A10a)}$$

$$-i\partial_\tau \mathbf{H}_P = \varepsilon_P \cdot \mathbf{E}_P - \nabla_p^{\perp}[(\nabla_p^{\perp} \cdot \mathbf{E}_P)/\mu] - \boldsymbol{\epsilon}_z' \epsilon_{zz}^{-1}(\nabla_p \cdot \mathbf{H}_P), \quad \text{(A10b)}$$

which can be easily rewritten in the matrix form (10) used in Sec. II.

[1] T. Todorov, N. Tomova, and L. Nikolova, Appl. Opt. **23**, 4309 (1984).
[2] F. Gori, Opt. Lett. **24**, 584 (1999).
[3] J. Tervo and J. Turunen, Opt. Lett. **25**, 785 (2000).
[4] J. Tervo and J. Turunen, Opt. Commun. **190**, 51 (2001).
[5] G. Cincotti, IEEE J. Quantum Electron. **39**, 1645 (2003).
[6] S. R. Nersisyan, N. V. Tabiryan, D. M. Steeves, and B. R. Kimball, J. Nonlinear Opt. Phys. Mater. **18**, 1 (2009).
[7] N. V. Tabiryan, S. R. Nersisyan, D. M. Steeves, and B. R. Kimball, Opt. Photonics News **21**, 40 (2010).
[8] L. Nikolova and P. S. Ramanujam, *Polarization Holography* (Cambridge University Press, Cambridge, 2009), p. 239.
[9] Z. Bomzon, V. Kleiner, and E. Hasman, Opt. Commun. **192**, 169 (2001).
[10] Z. Bomzon, G. Biener, V. Kleiner, and E. Hasman, Opt. Lett. **27**, 188 (2002).
[11] G. Biener, A. Niv, V. Kleiner, and E. Hasman, J. Opt. Soc. Am. A **20**, 1940 (2003).
[12] Y. Gorodetski, G. Biener, A. Niv, V. Kleiner, and E. Hasman, Opt. Lett. **30**, 2245 (2005).
[13] Z. Bomzon, G. Biener, V. Kleiner, and E. Hasman, Appl. Opt. **41**, 5218 (2002).
[14] Z. Bomzon, G. Biener, V. Kleiner, and E. Hasman, Opt. Lett. **27**, 1141 (2002).
[15] Y. Yirmiyahu, A. Niv, G. Biener, V. Kleiner, and E. Hasman, Opt. Lett. **31**, 3252 (2006).
[16] J. N. Eakin, Y. Xie, R. A. Pelcovits, M. D. Radcliffe, and G. P. Crawford, Appl. Phys. Lett. **85**, 1671 (2004).
[17] G. P. Crawford, J. N. Eakin, M. D. Radcliffe, A. Callan-Jones, and R. A. Pelcovits, J. Appl. Phys. **98**, 123102 (2005).
[18] V. Presnyakov, K. Asatryan, T. Galstian, and V. Chigrinov, Opt. Express **14**, 10558 (2006).
[19] C. Provenzano, P. Pagliusi, and G. Cipparrone, Appl. Phys. Lett. **89**, 121105 (2006).
[20] C. Provenzano, P. Pagliusi, and G. Cipparrone, Opt. Express **15**, 5872 (2007).
[21] H. Choi and J. W. Wu, J. Opt. Soc. Am. B **26**, 1 (2009).
[22] V. G. Chigrinov, V. M. Kozenkov, and H. S. Kwok, in *Optical Applications in Photoaligning* edited by L. Vicari (Institute of Physics, Bristol, UK, 2003), pp. 201–244.
[23] A. D. Kiselev, V. G. Chigrinov, and D. D. Huang, Phys. Rev. E **72**, 061703 (2005).
[24] V. G. Chigrinov, V. M. Kozenkov, and H.-S. Kwok, *Photoalignment of Liquid Crystalline Materials: Physics and Applications*, Series in Display Technology (Wiley, Chichester, 2008), p. 219.
[25] R. K. Komanduri and M. J. Escuti, Phys. Rev. E **76**, 021701 (2007).
[26] P. G. de Gennes and J. Prost, *The Physics of Liquid Crystals* (Clarendon Press, Oxford, 1993), p. 596.
[27] A. D. Kiselev, J. Phys. Condens. Matter **19**, 246102 (2007).
[28] A. D. Kiselev, R. G. Vovk, R. I. Egorov, and V. G. Chigrinov, Phys. Rev. A **78**, 033815 (2008).
[29] L. A. Beresnev, V. G. Chigrinov, D. I. Dergachev, E. P. Poshidaev, J. Fünfschilling, and M. Schadt, Liq. Cryst. **5**, 1171 (1989).
[30] V. G. Chigrinov, *Liquid Crystal Devices: Physics and Applications* (Artech House, Boston, 1999), p. 357.
[31] N. A. Clark and S. T. Lagerwall, Appl. Phys. Lett. **36**, 899 (1980).
[32] I. Abdulhalim and G. Moddel, Mol. Cryst. Liq. Cryst. **200**, 79 (1991).
[33] E. Pozhidaev, S. Pikin, D. Ganzke, S. Shevtchenko, and W. Haase, Ferroelectrics **246**, 1141 (2000).
[34] G. B. Cohen, R. Pogreb, K. Vinokur, and D. Davidov, Appl. Opt. **3**, 455 (1997).
[35] G. Hedge, P. Xu, E. Pozhidaev, V. Chigrinov, and H. S. Kwok, Liq. Cryst. **35**, 1137 (2008).
[36] P. Kuchment, *Floquet Theory for Partial Differential Equations*, Operator Theory, Advances and Applications, Vol. 60 (Birkhäuser Verlag, Boston, 1993), p. 350.
[37] E. P. Pozhidaev, S. I. Torgova, V. E. Molkin, M. V. Minchenko, V. V. Vashchenko, A. I. Krivoshey, and A. Strigazzi, Mol. Cryst. Liq. Cryst. **509**, 1042 (2009).
[38] E. Pozhidaev, V. Chigrinov, D. Huang, A. Zhukov, J. Ho, and H. S. Kwok, Jpn. J. Appl. Phys. **43**, 5440 (2004).
[39] E. Pozhidaev, V. Chigrinov, and L. Xihua, Jpn. J. Appl. Phys. **45**, 875 (2006).
[40] E. Pozhidaev, S. Torgova, M. Minchenko, C. A. R. Yednak, A. Strigazzi, and E. Miraldi, Liq. Cryst. **37**, 1067 (2010).
[41] A. D. Kiselev, V. G. Chigrinov, and H.-S. Kwok, Phys. Rev. E **80**, 011706 (2009).
[42] A. D. Kiselev and R. G. Vovk, JETP **110**, 901 (2010).
[43] E. Pozhidaev, A. Bobrovsky, V. Shibaev, G. Elyashevich, and M. Minchenko, Liq. Cryst. **37**, 517 (2010).
[44] M. Nevière and E. Popov, *Light Propagation in Periodic Media: Differential Theory and Design*, Optical Engineering, Vol. 81 (Dekker, New York, 2003), p. 410.
[45] E. Popov and M. Neviére, J. Opt. Soc. Am. A **18**, 2886 (2001).
[46] L. Li, J. Opt. A: Pure Appl. Opt. **5**, 345 (2003).
[47] G. Kreymerman, Opt. Express **18**, 15513 (2010).
[48] V. G. Chigrinov, V. A. Baikalov, E. P. Pozhidaev, L. M. Blinov, L. A. Beresnev, and A. I. Allagulov, Sov. Phys. JETP **61**, 1193 (1985).
[49] C. Oh and M. J. Escuti, Phys. Rev. A **76**, 043815 (2007).
[50] S. Suwa, H. Hoshi, Y. Takanishi, K. Ishikawa, H. Takezoe, and B. Zeks, Jpn. J. Appl. Phys. **42**, 1335 (2003).